Journal of Magnetism and Magnetic Materials 526 (2021) 167759

Contents lists available at ScienceDirect

Journal of Magnetism and Magnetic Materials

journal homepage: www.elsevier.com/locate/jmmm

Research articles

Cluster glass characteristics of disordered La_2CuMnO_6 double perovskite oxides

Md. G. Masud [a,*], S. Giri [b]

[a] Department of Physics, Basanti Devi College, 147B Rash Behari Avenue, Kolkata 700 029, India
[b] School of Physical Sciences, Indian Association for the Cultivation of Science, Jadavpur, Kolkata 700 032, India

ARTICLE INFO

Keywords:
Oxides
X-Ray diffraction
Double perovskite
Magnetic properties

ABSTRACT

The structural and magnetic properties of disordered La_2CuMnO_6 double perovskite oxide are reported. Temperature variation of dc magnetization in zero field cooled and field cooled protocols manifest the cluster glass feature of the compound. The cooperative glassy magnetic state is explored by the memory effect in thermal variation as well as relaxation dynamics. The frequency dependent shift of the ac susceptibility peak satisfies dynamical scaling law with $T_c \sim 26.4$ K and dynamic exponent $z\nu \sim 3.26$ proposing a cluster-glass like state. The anti-site disorder and competing exchange interactions of two different transition metal have been argued for the observed cluster glass state in this B-site disordered La_2CuMnO_6 double perovskite.

1. Introduction

Perovskites and related perovskite-like materials [1–3] are remarkably interesting class of inorganic materials whose properties were actively investigated for decades [4–8]. Prototypical ABO_3 perovskite compounds (A = alkaline earth or rare-earth metal, B = transition metals) is characterized by a three-dimensional framework made up of BO_6 octahedra [1,2]. The larger A cations occupy the interstices formed by the corner sharing octahedral of oxygen anions. There are other set of compounds in the family of perovskite like crystals whose structures retain the most important feature of perovskites - like the presence of frameworks, layers, or networks of BO_6 octahedra, BO_5 pyramids and BO_4 squares linked at their vertices [2]. One of such system is ordered perovskites or double perovskite $A_2BB'O_6$, where the $(B/B')O_6$ octahedra alternate in all the three directions. Double perovskite compounds with general formula $A_2BB'O_6$, have attracted a lot of attention in recent years due to a variety of dielectric, magnetic and magnetoelectric properties exhibited by them [9,10]. Depending on the choice of B and B′ cations, these compounds show vast variety of electrical and magnetic properties; namely, metallicity [11], half-metallicity [12], insulating as well as ferromagnetism [13], ferrimagnetism [14], antiferromagnetic [15], large magnetocapacitance [13,16], magnetoresistance [17], and strong spin phonon coupling [18] etc.

In the current investigation we focus on a hitherto less explored compound La_2CuMnO_6. We observe spin-glass characteristics of the compound at low temperature. Though, electrical modulus scaling were carried out [19] and interesting magnetodielectric behaviour is also reported [20] for La_2CuMnO_6. In this article, we explore the dc magnetometry and ac susceptibility results at low temperature and propose a new observation of spin-glass like transition close to 26 K, which has not been reported to the best of our knowledge. The spin-glass like behaviour observed in La_2CuMnO_6 has been correlated to the anti-site disorder and competing magnetic interactions.

Polycrystalline La_2CuMnO_6 was prepared by standard solid-state reaction route from a stoichiometric mixture of La_2O_3, CuO and MnO_2. The crystalline structure was investigated by X-ray powder diffraction (XRD-Bruker D8 Advance) using Cu-K_α radiation. Magnetization measurements were made in a superconducting quantum interference device (SQUID, EverCool) magnetometer and Physical Properties Measuring System (PPMS, Cryogenics, UK).

2. Results and discussion

X-ray powder diffraction pattern at 300 K is shown in Fig. 1. The diffraction could be fitted to both the orthorhombic Pnma and monoclinic $P2_1/n$ space group. In monoclinic $P2_1$ /n space group, the two different transition metal cations (Cu and Mn) are ordered in checkerboard pattern at the Wyckoff '2c' and '2d' sites. In contrast, the cations are randomly distributed in orthorhombic Pnma space group. However, keeping in mind the partial disorder nature observed [21,22] in other

* Corresponding author.
E-mail addresses: physics.masud@gmail.com (Md.G. Masud), sspsg2@gmail.com (S. Giri).

https://doi.org/10.1016/j.jmmm.2021.167759
Received 10 July 2020; Received in revised form 6 January 2021; Accepted 10 January 2021
Available online 22 January 2021

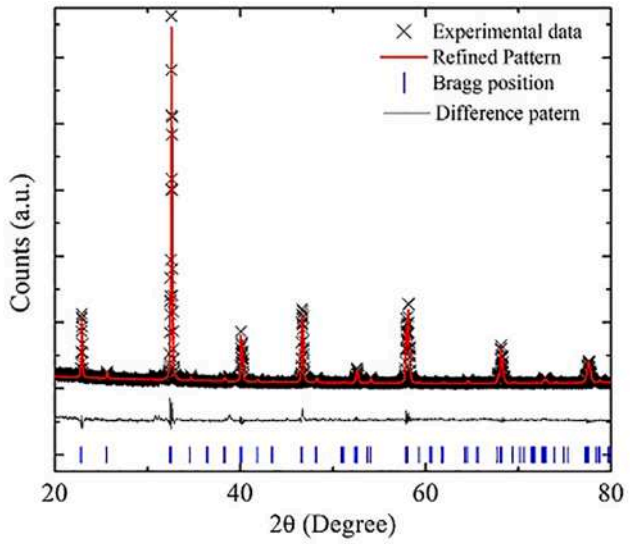

Fig. 1. X-ray diffraction pattern at 300 K. The observed (black cross), calculated (red line), and difference (bottom black continuous line) patterns are shown. The Bragg reflections are also indicated by blue tick marks.

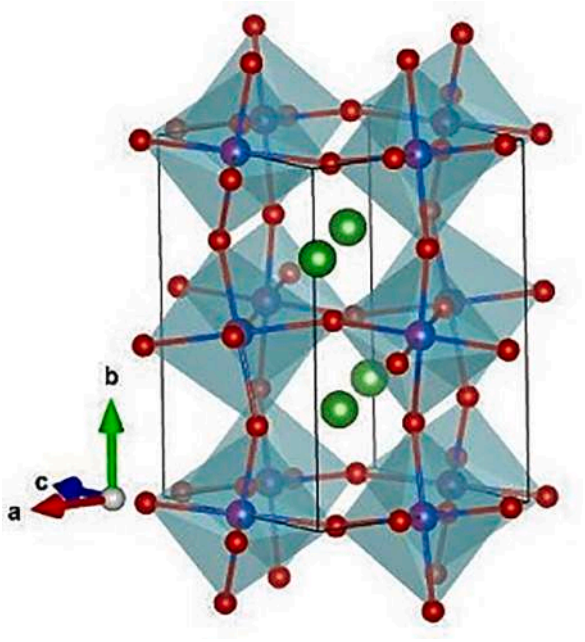

Fig. 2. Orthorhombic Pnma double perovskite crystal structure of La_2CuMnO_6, showing the tilted oxygen octahedra surrounding disordered Cu and Mn cations. Oxygen ions are small red dots at the corners of the octahedra, and La ions are the largest green balls existing at interstial sites between the octahedra.

double perovskite viz La_2NiMnO_6; the observed X-ray diffraction pattern were refined with orthorhombic Pnma space group. The refinement is shown in Fig. 1, demonstrating a reasonable fitting with such prescription. The lattice parameters, bond lengths and reliability factors of the refinement are tabulated in table 1. Using refined structural parameters, a crystal structure is drawn in Fig. 2. The TM-O-TM (TM = Cu/Mn) bond angles deviates appreciably from linear 180° situation. The lattice parameters are found larger with respect to *iso*-structural La_2NiMnO_6 and La_2CoMnO_6 double perovskite [22].

Thermal variations of magnetization recorded in field cooled, zero field cooled protocols along with the thermoremanent magnetization are presented in Fig. 3. In the standard field cooled (FC) approach, the sample is cooled from 298 K in 0.5 kOe, where measurements were performed during cooling process, defined as field cooled cooling (FCC). The temperature was then increased with the field and measurement was carried out during warming, defined as field cooled warming (FCW). During zero field cooled (ZFC) procedure, the sample was cooled from 298 K down to 4 K in the absence of field, thereafter the magnetization is measured with increasing temperature in 0.5 kOe. Fig. 3

Table 1
Structural and reliability parameters obtained from the refinement for the double perovskite La_2CuMnO_6.

Lattice Parameters (Å)			
a(Å)		5.493	
b(Å)		7.780	
c(Å)		5.527	
Bond Length (Å)			
TM-O1		2.002	
TM-O2		1.925	
Bond Angles (Degree)			
TM-O1-TM		152.5 (4)	
TM-O2-TM		161.4(4)	
Atoms	**x**	**y**	**z**
La	0.0221	0.2	−0.0059
Cu	0	0	0.5
Mn	0	0	0.5
O1	0.478	0.25	0.0832
O2	0.280	0.0331	0.732
Reliability factor			
Rw		9.776	
Rwnb		6.860	
Rb		7.524	
σ		1.709	

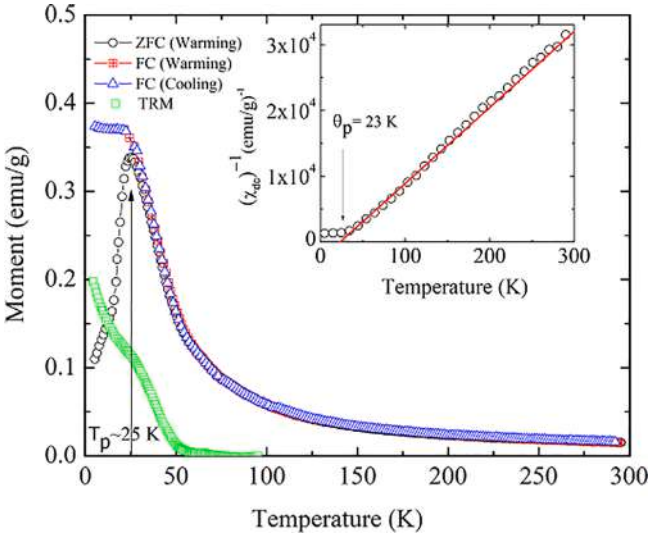

Fig. 3. Temperature (*T*) dependent magnetization (*M*) measured under different protocols described in the text. Inset shows the inverse of dc magnetic susceptibility as a function of temperature along with Curie-Wiess fit.

illustrates temperature dependence of ZFC, FCC and FCW magnetization. The ZFC magnetization exhibits a peak around 25 K (T_p). The FC magnetization deviates from ZFC magnetization close to T_p. Below T_p, a broadened maximum in FC magnetization is observed as shown in the figure, which is a usual characteristic feature of spin-glasses [23–26]. Inset of the Fig. 3 depicts thermal variation of the inverse dc susceptibility following Curie-Weiss law in the high temperature region. The Curie temperature and the effective paramagnetic moment are ~ 23 K and ~ 5.73μ_B, respectively. The effective paramagnetic Curie moment is well correlated to the theoretical value of effective magnetic moment 5.60μ_B for the magnetic moment of Cu^{2+} and Mn^{4+} ions. The estimate of paramagnetic moment in higher temperature could give much better

agreement with the theoretical calculation. The thermoremanent magnetization (TRM) as a function of temperature is also shown in Fig. 3. During the TRM measurement, the system was cooled from 298 K down to 4 K in 0.5 kOe, subsequently the field was turned off and the magnetization was measured with increasing temperature. The observed TRM gradually decreases with increasing temperature and started to appear much higher than T_p, indicating a shoulder close to T_p. Fig. 4 shows the magnetization curves M(H) at selected temperatures. At 5 K the curve does not show saturation of magnetization at 50 kOe. The value of coercivity is 0.16 kOe at 5 K. A nonlinear M(H) still exists much above T_p at 50 K. As expected, a linear M(H) is observed in the paramagnetic region at 300 K.

To confirm spin-glass like state below T_p, the experiment on memory effect is carried out both in ZFC and FC protocols. The protocols used here are identical to that adopted by sun *et al* [27]. For FC protocol, the sample was first cooled in 0.5 kOe from 200 K down to 4 K at a constant cooling rate of 2 K/min. The sample is heated back continuously at the same rate and the magnetization is recorded. The obtained M−T curve is referred to as the reference curve (FC ref) and is shown as a dashed line in Fig. 5(a). The sample is then cooled at the same rate again and the magnetization is recorded during cooling with temporarily stops at three different temperatures, T_s = 22, 14 and 7 K, respectively for a waiting time, t_w = 1 h, respectively. During t_w, the field is also cut off and magnetization is set to relax. After each stop and wait period, the 0.5 kOe field is re-applied and measurement is resumed during cooling process. This brings out sharp steps in M−T curve [FCC (IS), IS = intermittent stop] as shown by the red open circle in Fig. 5(a). After reaching the base temperature at 4 K, the sample temperature is raised continuously at a rate of 2 K/min in 0.5 kOe as shown by the blue open symbols (FCH curve). Although measurement is done continuously, an evident signature of steps close to the stop temperatures is observed, demonstrating the memory effect in FC protocol. Observation of memory effect in FC protocol may appear due to extrinsic effect, as pointed out for the magnetic nanoparticles [28]. In order to confirm memory effect further, ageing process was investigated in ZFC protocol also. The sample was first cooled in zero magnetic field from 100 K down to a stop temperature T_s = 20 K. The system was aged at T_s for a wait time t_s = 1 h. Further cooling is then resumed down to 2 K. Magnetization is then measured in warming cycle with 0.1 kOe. In Fig. 5(b) the black square symbols depict the ZFC memory curve [ZFC (IS)] and the results are compared with the reference ZFC curve [ZFC (ref)] as depicted by the red open circles. An evident signature of dip is observed around 20 K, at which sample was halted during the cooling cycle. The memory effect in ZFC magnetization confirms spin glass like characteristics [29,30].

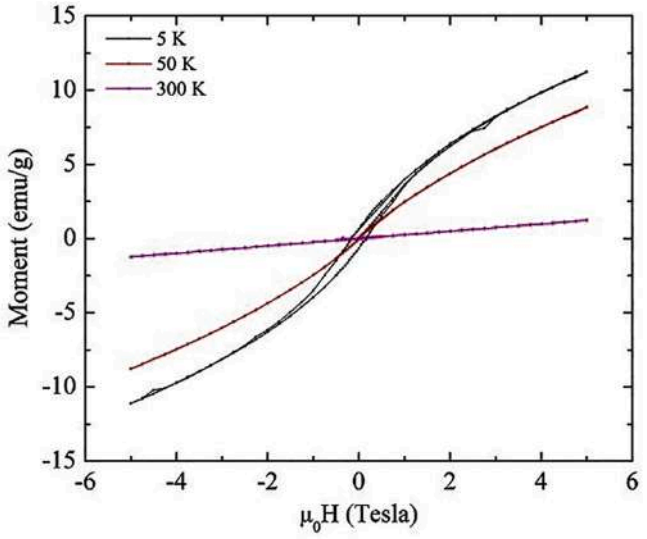

Fig. 4. (a) Isothermal magnetization curves recorded from + 50 to −50 kOe at selected temperature.

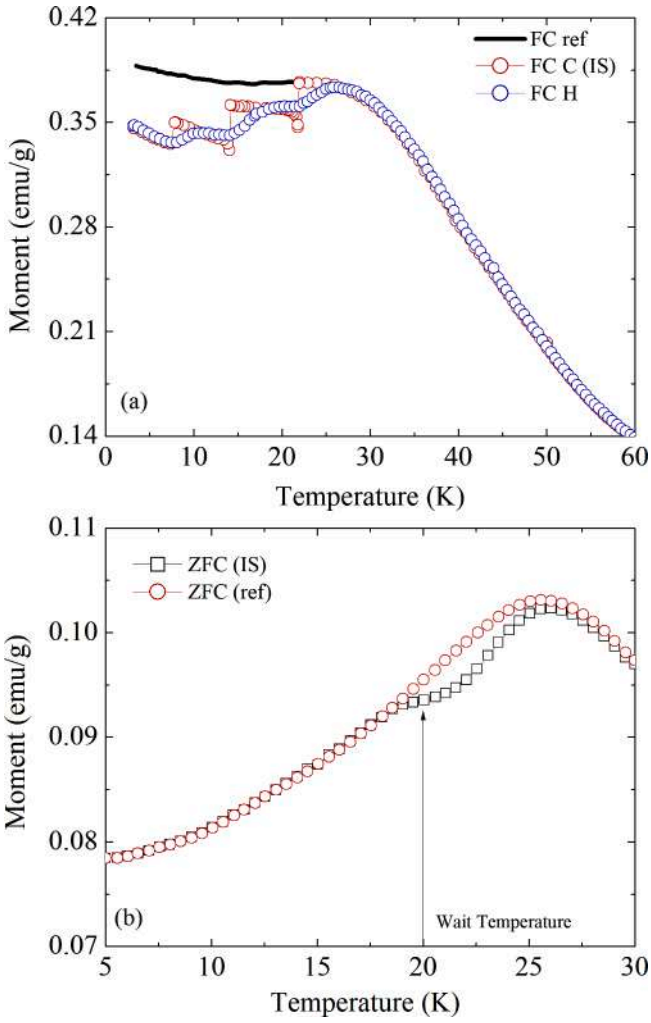

Fig. 5. (a) Memory effect in the dc magnetization. The reference curve (dashed black line) is measured on heating at a constant rate of 2 K/min after FC in 0.5 kOe. The open red circles are measured during cooling in 0.5 kOe at the same rate, but with stops of 1 h duration at 22, 14, and 7 K. The field is cut off during each stop temperatures. The blue open circles are measured with continuous heating at the same rate after the previous cooling procedure. (b) The memory effect in the temperature dependence of the zero-field cooled magnetization in the 0.1 kOe field. Red open circle and black square represents the reference M_{ref} (ZFCW) and memory curves M_{mem}(ZFCW), respectively.

Memory effect is further studied during field and temperature cycling in the relaxation dynamics for both the FC and ZFC mode. The result of the experiment is shown in Fig. 6. In the FC mode (shown in Fig. 6(a), the sample is cooled down to 15 K in 0.1 kOe magnetic field. After stabilizing the temperature, field is turned off and magnetization is recorded with time (t) for 1 h (t_1). The sample temperature is then decreased to 10 K and the magnetization is recorded with t in field of 0.1 kOe for 1 h (t_2). The system is again returned to 15 K in zero field and the magnetization relaxation is measured for 1 h (t_3) in zero field. Analogous to the field-cooled measurement, memory effect in relaxation dynamics measured for ZFC is described in Fig. 6(b). In both the ZFC and FC protocols intermediate cooling followed by the waiting in field and zero field, respectively does not influence the elapse of magnetization even for t_3 time period, as indicated by the continuous curves in Fig. 6. These results further demonstrate the memory effect.

Time evolution of magnetization is investigated below T_p at selected

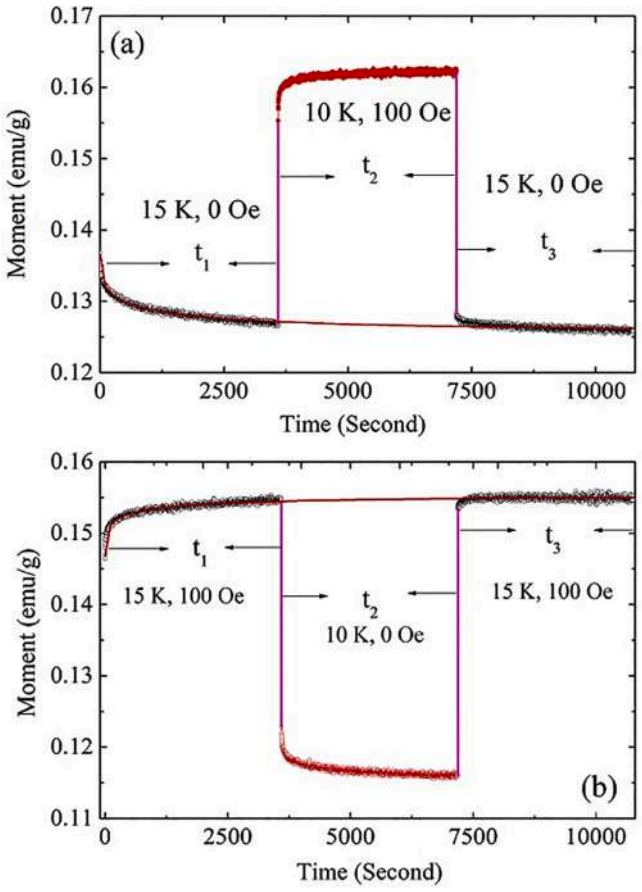

Fig. 6. (a) Magnetic relaxation at 15 K and in zero field for t_1 and t_3 after cooling in FC mode with an intermediate measurement at 10 K in 0.1 kOe for t_2. (b) Magnetic relaxation at 15 K in 0.1 kOe for t_1 and t_3 after ZFC with an intermediate cooling and measurement at 10 K for t_2 in zero field. Continuous curves in (a) and (b) display the fit using stretched exponential function.

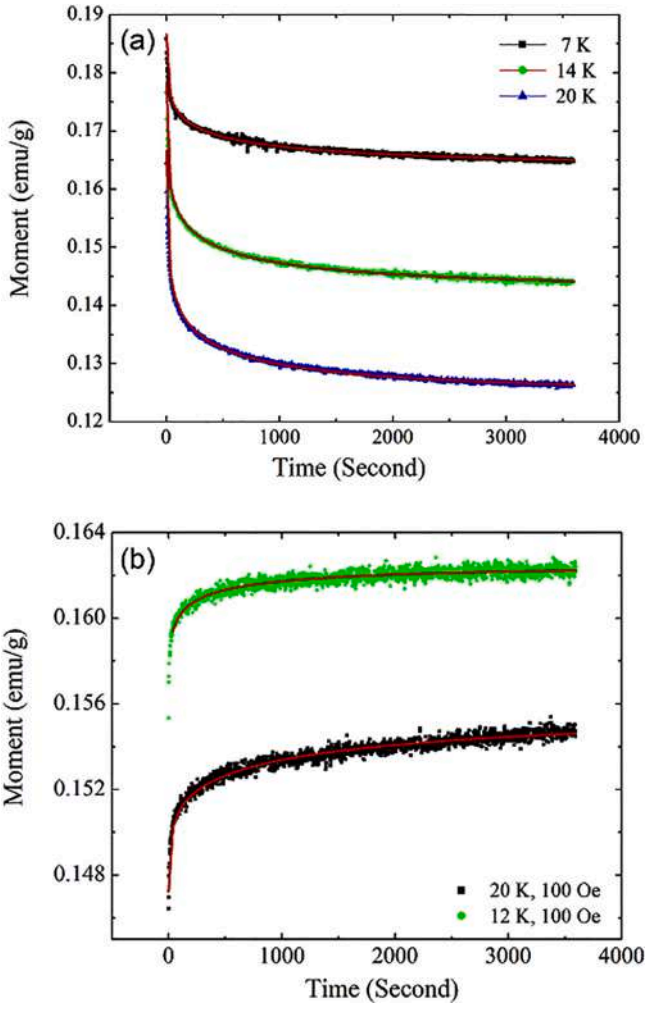

Fig. 7. (a) Time (t) decay of magnetization at selective temperatures (a) in zero field after field cooling (0.1 kOe) and (b) in 0.1 kOe after zero field cooling. Continuous curves depict the fit using stretched exponential function.

temperatures both in ZFC and FC protocols. In FC protocol sample is cooled in field (0.1 kOe) and relaxation of magnetization is recorded in zero field and for ZFC protocol sample is cooled in zero field and measurement is carried out in field (0.1 kOe). The results are depicted in Fig. 7(a) and 7(b). Magnetization as a function of time for all cases can be described well with the stretched exponential function [31,32] given by:

$$M(t) = M_0 - M_g \exp\left(-\frac{t}{\tau}\right)^{\beta} \quad (1)$$

where M_0 and M_g are related to an initial remnant magnetization required to fit the decay of magnetization, and to a glassy component of the magnetization, respectively. β is an exponent which lies in the range $0 < \beta \leq 1$. In all the cases, the fit provides the value of beta in between 0.3 and 0.32 (0.3, 0.3 and 0.32 at 7, 14 and 20 K respectively in Fig. 7(a). The corresponding value at 12 and 20 K in 7(b) turned out to be 0.3 and 0.31, respectively). The observed value of $\beta < 1$ signifies that the system evolves through a number of intermediate states where activation takes place against multiple anisotropic barriers as expected for spin glasses [30].

To characterize spin-glass like behaviour, thermal variation of ac susceptibility is measured at different frequencies (f). The results around T_p is depicted in Fig. 8 for f = 3, 17, 93, and 297 Hz. The peak position shifts toward high temperature whereas peak height decreases with increasing f. This dependence of T_f on f is well described by the

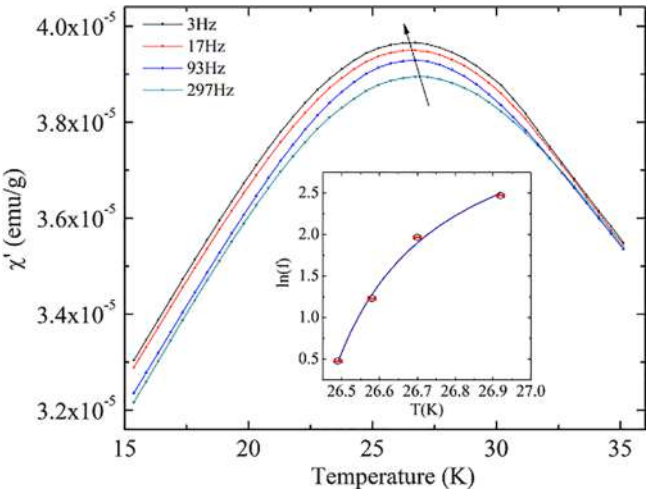

Fig. 8. (a) Temperature (T) variation of ac susceptibility (χ') at different frequencies (f). Inset shows the peak temperature (T_F) with frequency obeying the dynamical scaling law as described by Eq. (2).

conventional critical slowing down of the spin dynamics described by:

$$f = f_0 \zeta^{z\nu} \quad (2)$$

where $\zeta = (T_f - T_c)/T_f$, f_0 is the microscopic flipping time or attempt frequency, $z\nu$ is the dynamic exponent, T_f is the frequency dependent freezing temperature determined by the maximum in ac susceptibility and T_c provides the dc value of T_f for $f \to 0$. The best fit to Eq. (2) shown in the inset of Fig. 8 provides $T_c \sim 26.4$ K, $f_0 \sim 10^8$ Hz and $z\nu \sim 3.26$, respectively. The T_c is close to the peak observed in dc magnetization. The value of $z\nu$ is found to be smaller than that observed for classical spin glasses [23] in the range 4–12. The value of f_0 is significantly smaller than the range, 10^{12} –10^{14} Hz, usually observed for classical spin-glasses [23]. These results are in accordance with the frequency sensitivity [23] defined by: $K = \Delta T_f/[T_f \Delta(log\omega)]$ and propose the cluster-glass state below T_c. The frequency sensitivity has widely been used as a possible distinguishing feature of the spin glass (SG) phase from the superparamagnetic (SPM) state. In particular, the frequency sensitivity offers a good criterion for distinguishing SG's (<0.06) from SPM's (>0.3). The calculated value of K turns out to be ~ 0.02 which is slightly higher than conventional spin glass but much smaller than super paramagnet. Thus, frequency dependent ac susceptibility result proposes the cluster-glass state at low temperature.

3. Conclusion

Memory experiments in the thermal variations and relaxation dynamics suggest a spin-glass like behaviour in La_2CuMnO_6. Frequency dependence of the ac susceptibility result further indicates the cluster-glass like state at low temperature. In double perovskite, cation ordering is nucleated at different centres in the crystal. These ordered regions grow until they meet one another at an interface. The interfaces between differently ordered regions form antiphase boundaries or anti-site disorder. These anti-site disorder with an interchange between Cu and Mn sites has important consequences on the physical properties. Anti-site disorder leads to competing ferromagnetic (Cu^{2+}-O-Mn^{4+}) and antiferromagnetic (Mn^{4+}-O-Mn^{4+}, Cu^{2+}-O-Cu^{2+}) interactions. Hence, the observed spin glass like behaviour in the present study is well corelated to anti-site disorder introduced by frustrated and random distribution of ferromagnetic and antiferromagnetic interactions, which in turn lead to the spin glass like state at low temperature. Finally, we would like to emphasize that the nature of order and disorder of Cu and Mn cations can't be definitively studied with X-ray diffraction as the two TM cation have very similar scattering cross sections. In contrast, their neutron diffraction cross sections are quite different, and therefore such a neutron diffraction study is the suggested route for shedding light of such short-range order.

Declaration of Competing Interest

The authors declare that they have no known competing financial interests or personal relationships that could have appeared to influence the work reported in this paper.

Acknowledgments

MGM gratefully acknowledge different central facilities, and other measurement facilities obtained at Indian Association for the cultivation of Science (IACS), Kolkata. Prof. A Ghosh of IACS is gratefully acknowledged for his kind help during the magnetic measurement.

References

[1] R.H. Mitchell, T. Bay, *Perovskites: Modern and Ancient*, Almaz Press, Ontario, 2002.
[2] K.S. Aleksandrov, V.V. Beznosikov, Phys. Solid State 39 (1997) 695.
[3] Z.L. Wang, C.Z. Kang, Perovskite and related structure system. *Functional and Smart Materials-Structural Evolution and Structure Analysis* Chapter 3, Plenum Press, New York, 1998.
[4] J.B. Goodenough, Rep. Prog. Phys. 67 (2004) 1915.
[5] J.M.D. Coey, M. Viret, S. von Molnar, Adv. Phys. 48 (2) (1999) 167.
[6] A. Kulkarni, F.T. Ciacchi, S. Giddey, C. Munnings, et al., Int. J. Hydrogen Energy 37 (2012) 19092.
[7] G. Hodes, Science 342 (6156) (2013) 317.
[8] M. Liu, M.B. Johnston, H.J. Snaith, Nature 501 (2013) 395.
[9] S. Garcia, L.G. Fernández, I. Felner, L. Ghivelder, J. Magn. and Magn. Mater. 494 (2020), 165780.
[10] R.P. Madhogaria, E.M. Clements, V. Kalappattil, M.H. Phan, H. Srikanth, R. Das, N. T. Dang, D.P. Kozlenko, N.S. Bingham, J. Magn. and Magn. Mater. 507 (2020), 166821.
[11] G. Zhang, Y. Wang, Z. Cheng, Y. Yan, C. Peng, C. Wang, S. Dong, Phys. Chem. Chem. Phys. 17 (2015) 12717.
[12] K.C. Weng, Y.K. Wang, J. Appl. Phys. 117 (2015) 17D716.
[13] N.S. Rogado, J. Li, A.W. Sleight, M.A. Subramanian, Adv. Mater. 17 (2005) 2225.
[14] H. Wang, S. Zhu, X. Ou, H. Wu, Phys. Rev. B 90 (2014), 054406.
[15] Y. Izumiyama, Y. Doi, M. Wakeshima, Y. Hinatsu, Y. Shimojo, Y. Morii, J. Phys.: Condens. Matter 13 (2001) 130.
[16] M.G. Masud, A. Ghosh, J. Sannigrahi, B.K. Chaudhuri, J. Phys.: Condens. Matter. 24 (2010), 295902.
[17] K.I. Kobayashi, T. Kimura, H. Sawada, K. Terakura, Y. Tokura, Nature 395 (1998) 677.
[18] R.B.M. Filho, A.P. Ayala, C.W.A. Paschoa, Appl. Phys. Lett. 102 (2013), 192902.
[19] J.P. Palakkal, C. RajSankar, A.P. Paulose, M. Valant, M.R. Varma, Mat. Res. Bull. 100 (2018) 226–233.
[20] D.N. Singh, T.P. Sinha, D.K. Mahato, J. of Alloys and Comp. 729 (2017) 1226.
[21] D. Choudhury, P. Mandal, R. Mathieu, A. Hazarika, S. Rajan, A. Sundaresan, U. V. Waghmare, R. Knut, O. Karis, P. Nordblad, D.D. Sarma, Phys. Rev. Lett. 108 (2012), 127201.
[22] C.L. Bull, D. Gleeson, K.S. Knight, J. Phys.: Condens. Matter 15 (2003) 4927.
[23] J.A. Mydosh, Spin Glasses: An Experimental Introduction, Taylor and Francis, London, 1993.
[24] D. De, A. Karmakar, M.K. Bhunia, A. Bhaumik, S. Majumdar, S. Giri, J. Appl. Phys. 111 (2012), 033919.
[25] M. Thakur, M. Patra, S. Majumdar, S. Giri, J. Appl. Phys. 105 (2009) 3905.
[26] R. Borah, S. Ravi, J. Magn. and Magn. Mater. 502 (2020), 166550.
[27] Y. Sun, M.B. Salamon, K. Garnier, R.S. Averback, Phys. Rev. Lett. 91 (2003), 167206.
[28] D. De, K. Dey, S. Majumdar, S. Giri, Solid State Commun. 152 (2012) 1857.
[29] M. Sasaki, P.E. Jhonsson, H. Takayama, H. Mamiya, Phys. Rev. B 71 (2005), 104405.
[30] N. Khan, P. Mandal, D. Prabhakaran, Phys. Rev. B 90 (2014), 024421.
[31] J.C. Phillips, Rep. Prog. Phys. 59 (1996) 1133.
[32] R.V. Chamberlin, G. Mozurkewich, R. Orbach, Phys. Rev. Lett. 52 (1984) 867.